Runge-Kutta discontinuous Galerkin method using a new type of WENO limiters on unstructured meshes[1]

Jun Zhu[2], Xinghui Zhong[3], Chi-Wang Shu[4] and Jianxian Qiu[5]

Abstract

In this paper we generalize a new type of limiters based on the weighted essentially non-oscillatory (WENO) finite volume methodology for the Runge-Kutta discontinuous Galerkin (RKDG) methods solving nonlinear hyperbolic conservation laws, which were recently developed in [32] for structured meshes, to two-dimensional unstructured triangular meshes. The key idea of such limiters is to use the entire polynomials of the DG solutions from the troubled cell and its immediate neighboring cells, and then apply the classical WENO procedure to form a convex combination of these polynomials based on smoothness indicators and nonlinear weights, with suitable adjustments to guarantee conservation. The main advantage of this new limiter is its simplicity in implementation, especially for the unstructured meshes considered in this paper, as only information from immediate neighbors is needed and the usage of complicated geometric information of the meshes is largely avoided. Numerical results for both scalar equations and Euler systems of compressible gas dynamics are provided to illustrate the good performance of this procedure.

Key Words: Runge-Kutta discontinuous Galerkin method, limiter, WENO finite volume methodology

AMS(MOS) subject classification: 65M60, 35L65

[1]The research of J. Zhu and J. Qiu were partially supported by NSFC grant 10931004,11002071, 91230110 and and ISTCP of China Grant No. 2010DFR00700. The research of X. Zhong and C.-W. Shu were partially supported by DOE grant DE-FG02-08ER25863 and NSF grant DMS-1112700.

[2]College of Science, Nanjing University of Aeronautics and Astronautics, Nanjing, Jiangsu 210016, P.R. China. E-mail: zhujun@nuaa.edu.cn

[3]Department of Mathematics, Michigan State University, East Lansing, MI 48824, USA. E-mail: zhongxh@math.msu.edu

[4]Division of Applied Mathematics, Brown University, Providence, RI 02912, USA. E-mail: shu@dam.brown.edu

[5]School of Mathematical Sciences, Xiamen University, Xiamen, Fujian 361005, P.R. China. E-mail: jxqiu@xmu.edu.cn

1 Introduction

The discontinuous Galerkin (DG) method, initialized in 1973 by Reed and Hill [23], is one of the popular choices for solving conservation laws, the two-dimensional version studied in this paper being given by

$$\begin{cases} u_t + f(u)_x + g(u)_y = 0, \\ u(x, y, 0) = u_0(x, y). \end{cases} \tag{1.1}$$

For nonlinear time dependent equations such as (1.1), the so-called Runge-Kutta DG (RKDG) method developed in [6, 5, 4, 7] is particularly convenient to implement. The RKDG methods use explicit, nonlinearly stable high order Runge-Kutta methods [28] to discretize the temporal variable and the DG discretization to discretize the spatial variables, with exact or approximate Riemann solvers as interface fluxes. In this paper we consider only the RKDG methods for solving (1.1) on two-dimensional unstructured triangular meshes. For a detailed discussion on DG methods for solving conservation laws, we refer to the review paper [8] and the books and lecture notes [3, 12, 16, 27].

One of the main difficulties in using RKDG methods to solve (1.1) with possibly discontinuous solutions is that the numerical solution may be oscillatory near discontinuities. These spurious oscillations are not only unpleasant in appearance, they may also lead to nonlinear instability (for example the appearance of negative density or pressure for Euler equations) and eventual blow up of the codes. Therefore, it is important to investigate nonlinear limiters which are easy to implement, can remove or reduce such spurious oscillations near discontinuities, yet can still maintain the original high order accuracy of the RKDG methods. Many limiters have been studied in the literature on RKDG methods. For example, we mention the *minmod* type total variation bounded (TVB) limiter [6, 5, 4, 7], which is a slope limiter using a technique borrowed from the finite volume methodology [25]; the moment based limiter [1] and an improved moment limiter [2], which are specifically designed for discontinuous Galerkin methods to work on the moments of the numerical solution. One disadvantage of these limiters is that they may degrade accuracy when mistakenly used in

smooth regions of the solution.

In [19, 20, 22, 32, 33, 34], the weighted essentially non-oscillatory (WENO) finite volume methodology [17, 14, 10, 13] is used as limiters for the RKDG methods. The original WENO schemes were designed based on the successful ENO schemes in [11, 28, 29]. Both ENO and WENO schemes use the idea of adaptive stencils in the reconstruction procedure based on the local smoothness of the numerical solution to automatically achieve high order accuracy and a non-oscillatory property near discontinuities. The general framework in using the WENO methodology as limiters for RKDG methods is as follows:

Step 1: First, identify the troubled cells, namely those cells which might need the limiting procedure.

Step 2: Then, in any troubled cell, replace the solution polynomial by another reconstructed polynomial using the WENO procedure and information from both the target troubled cell and its neighboring cells, while maintaining the original cell average for conservation.

Study on Step 1 has been carried out in, e.g. [21]. The emphasis of this paper is not on Step 1, hence we will simply used one of the recommended techniques in [21], namely the KXRCF technique [15], to identify troubled cells in this paper. Other troubled cell indicator techniques can of course also be used. We emphasize that, if the limiter in Step 2 can retain the original high order accuracy of the RKDG scheme, then a non-optimal performance in Step 1, as long as it does not miss real shocked cells, would only lead to additional computational cost (to perform Step 2 in troubled cells which actually correspond to smooth regions of the solution), but not a degradation of the order of accuracy.

In the previous work [20, 33, 34], the limited polynomial in a troubled cell is reconstructed based on the traditional WENO methodology, namely using the cell averages in a local stencil consisting of the troubled cell and some of its neighboring cells to reconstruct the point values at quadrature points or suitable moments of the approximation, and then to obtain the new reconstruction polynomial. This procedure tends to use a rather wide stencil, especially for higher order of accuracy, involving both immediate neighbors and neighbors' neighbors etc.

Also, the traditional WENO procedure is complicated for unstructured meshes [13, 31], with the possibility of negative linear weights and special treatments needed to handle them [24]. In [19, 22, 18], a Hermite WENO procedure is adopted, which uses not only the cell averages but also the first derivative or first order moment information in the stencil for the WENO reconstruction, thereby reducing the width of the reconstruction stencil. However, for higher order methods information from just the immediate neighbors is still not enough, and the appearance of negative linear weights is still a problem.

More recently, in [32], Zhong and Shu developed a new WENO limiting procedure for RKDG methods on structured meshes. The idea is to reconstruct the entire polynomial, instead of reconstructing point values or moments in the classical WENO reconstructions. That is, the entire reconstruction polynomial on the target cell is a convex combination of polynomials on this cell and its immediate neighboring cells, with suitable adjustments for conservation and with the nonlinear weights of the convex combination following the classical WENO procedure. The main advantage of this limiter is its simplicity in implementation, as it uses only the information from immediate neighbors and the linear weights are always positive. This simplicity is more prominent for multi-dimensional unstructured meshes, which will be studied in this paper. We generalize the technique in [32] to two-dimensional unstructured triangular meshes, and perform numerical experiments for both scalar equations and Euler systems of compressible gas dynamics.

This paper is organized as follows. We describe the details of this new procedure on two-dimensional triangular meshes for the second and third order DG methods in Section 2 and present extensive numerical results in Section 3 to verify the accuracy and stability of this approach. Concluding remarks are given in Section 4.

2 The new WENO limiter to the RKDG method on unstructured meshes

In this section, we describe the details of using the new WENO reconstruction procedure as a limiter for the RKDG method. This is a generalization to unstructured meshes of the procedure in [32] for structured meshes.

2.1 Review of the RKDG method on unstructured meshes

Given a triangulation consisting of cells $\triangle_j$, $\mathbb{P}^k(\triangle_j)$ denotes the set of polynomials of degree at most k defined on $\triangle_j$. Here k could actually change from cell to cell, but for simplicity we assume it is a constant over the whole triangulation. In the DG method, the solution as well as the test function space is given by $V_h^k = \{v(x,y) : v(x,y)|_{\triangle_j} \in \mathbb{P}^k(\triangle_j)\}$. We emphasize that the procedure described below does not depend on the specific basis chosen for the polynomials. We adopt a local orthogonal basis over a target cell, such as $\triangle_0$: $\{v_l^{(0)}(x,y), l = 0, \ldots, K; K = (k+1)(k+2)/2 - 1\}$:

$$
\begin{aligned}
v_0^{(0)}(x,y) &= 1, \\
v_1^{(0)}(x,y) &= \frac{x-x_0}{\sqrt{|\triangle_0|}}, \\
v_2^{(0)}(x,y) &= a_{21}\frac{x-x_0}{\sqrt{|\triangle_0|}} + \frac{y-y_0}{\sqrt{|\triangle_0|}} + a_{22}, \\
v_3^{(0)}(x,y) &= \frac{(x-x_0)^2}{|\triangle_0|} + a_{31}\frac{x-x_0}{\sqrt{|\triangle_0|}} + a_{32}\frac{y-y_0}{\sqrt{|\triangle_0|}} + a_{33}, \\
v_4^{(0)}(x,y) &= a_{41}\frac{(x-x_0)^2}{|\triangle_0|} + \frac{(x-x_0)(y-y_0)}{|\triangle_0|} + a_{42}\frac{x-x_0}{\sqrt{|\triangle_0|}} + a_{43}\frac{y-y_0}{\sqrt{|\triangle_0|}} + a_{44}, \\
v_5^{(0)}(x,y) &= a_{51}\frac{(x-x_0)^2}{|\triangle_0|} + a_{52}\frac{(x-x_0)(y-y_0)}{|\triangle_0|} + \frac{(y-y_0)^2}{|\triangle_0|} + a_{53}\frac{x-x_0}{\sqrt{|\triangle_0|}} \\
&\quad + a_{54}\frac{y-y_0}{\sqrt{\triangle_0}} + a_{55}, \\
&\cdots
\end{aligned}
$$

where (x_0, y_0) and $|\triangle_0|$ are the barycenter and the area of the target cell $\triangle_0$, respectively. Then we would need to solve a linear system to obtain the values of $a_{\ell m}$ by the orthogonality

property:

$$\int_{\triangle_0} v_i^{(0)}(x,y)\, v_j^{(0)}(x,y)\, dxdy = w_i \delta_{ij}, \tag{2.1}$$

with $w_i = \int_{\triangle_0} \left(v_i^{(0)}(x,y) \right)^2 dxdy$.

The numerical solution $u^h(x,y,t)$ in the space V_h^k can be written as:

$$u^h(x,y,t) = \sum_{l=0}^{K} u_0^{(l)}(t)\, v_l^{(0)}(x,y), \qquad \text{for } (x,y) \in \triangle_0,$$

and the degrees of freedom $u_0^{(l)}(t)$ are the moments defined by

$$u_0^{(l)}(t) = \frac{1}{w_l} \int_{\triangle_0} u^h(x,y,t)\, v_l^{(0)}(x,y) dxdy, \qquad l = 0, \cdots, K.$$

In order to determine the approximate solution, we evolve the degrees of freedom $u_0^{(l)}(t)$:

$$\begin{aligned} \frac{d}{dt} u_0^{(l)}(t) &= \frac{1}{w_l} \left(\int_{\triangle_0} \left(f(u^h(x,y,t)) \frac{\partial}{\partial x} v_l^{(0)}(x,y) + g(u^h(x,y,t)) \frac{\partial}{\partial y} v_l^{(0)}(x,y) \right) dxdy \right. \\ &\quad \left. - \int_{\partial \triangle_0} (f(u^h(x,y,t)), g(u^h(x,y,t)))^T \cdot n\; v_l^{(0)}(x,y)\, ds \right), \\ &\quad l = 0, \ldots, K. \end{aligned} \tag{2.2}$$

where $n = (n_x, n_y)^T$ is the outward unit normal of the triangle boundary $\partial \triangle_0$.

In (2.2) the integral terms can be computed either exactly or by suitable numerical quadratures which are exact for polynomials of degree up to $2k$ for the element integral and up to $2k+1$ for the edge integral. In this paper, we use A_G quadrature points ($A_G = 6$ for $k = 1$ and $A_G = 7$ for $k = 2$) for the element integrals and E_G Gaussian points ($E_G = 2$ for $k = 1$ and $E_G = 3$ for $k = 2$) for the edge integrals:

$$\begin{aligned} &\int_{\triangle_0} \left(f(u^h(x,y,t)) \frac{\partial}{\partial x} v_l^{(0)}(x,y) + g(u^h(x,y,t)) \frac{\partial}{\partial y} v_l^{(0)}(x,y) \right) dxdy \approx \\ &|\triangle_0| \sum_G \sigma_G \left(f(u^h(x_G, y_G, t)) \frac{\partial}{\partial x} v_l^{(0)}(x_G, y_G) + g(u^h(x_G, y_G, t)) \frac{\partial}{\partial y} v_l^{(0)}(x_G, y_G) \right) \end{aligned} \tag{2.3}$$

$$\begin{aligned} &\int_{\partial \triangle_0} (f(u^h(x,y,t)), g(u^h(x,y,t)))^T \cdot n\; v_l^{(0)}(x,y)\, ds \\ \approx\; &|\partial \triangle_0| \sum_G \bar{\sigma}_G \left(f(u^h(\bar{x}_G, \bar{y}_G, t)), g(u^h(\bar{x}_G, \bar{y}_G, t)) \right)^T \cdot n\; v_l^{(0)}(\bar{x}_G, \bar{y}_G) \Big), \end{aligned} \tag{2.4}$$

where $(x_G, y_G) \in \triangle_0$ and $(\bar{x}_G, \bar{y}_G) \in \partial\triangle_0$ are the quadrature points, and σ_G and $\bar{\sigma}_G$ are the quadrature weights. Since the edge integral is on element boundaries where the numerical solution is discontinuous, the flux $(f(u^h(x,y,t)), g(u^h(x,y,t)))^T \cdot n$ is replaced by a monotone numerical flux for the scalar case and by an approximate Riemann solver for the system case. The simple Lax-Friedrichs flux is used in all of our numerical tests. The semi-discrete scheme (2.2) is discretized in time by a non-linearly stable Runge-Kutta time discretization [28], e.g. the third-order version:

$$\begin{aligned} u^{(1)} &= u^n + \Delta t L(u^n), \\ u^{(2)} &= \frac{3}{4}u^n + \frac{1}{4}u^{(1)} + \frac{1}{4}\Delta t L(u^{(1)}), \\ u^{n+1} &= \frac{1}{3}u^n + \frac{2}{3}u^{(2)} + \frac{2}{3}\Delta t L(u^{(2)}). \end{aligned} \tag{2.5}$$

2.2 The troubled cell indicator

The method described above can compute solutions to (1.1), which are either smooth or have weak shocks and other discontinuities, without further modification. If the discontinuities are strong, however, the scheme will generate significant oscillations and even nonlinear instability. To avoid such difficulties, we apply a nonlinear WENO limiter after each Runge-Kutta inner stage to control the numerical solution. The main focus of this paper is the development of a new, simple WENO limiter for unstructured meshes.

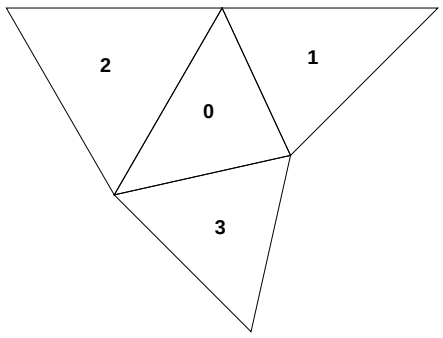

Figure 2.1: The stencil $S = \{\triangle_0, \triangle_1, \triangle_2, \triangle_3\}$

In the following, we relabel the target cell and its neighboring cells as shown in Figure 2.1. This forms the stencil of the WENO reconstruction. We then use the KXRCF shock detection technique developed in [15] to detect troubled cells. We divide the boundary of the target cell $\triangle_0$ into two parts: $\partial\triangle_0^+$ and $\partial\triangle_0^-$, where the flow is into ($v \cdot n < 0$) and out of ($v \cdot n > 0$) $\triangle_0$ respectively. Here we define v, taking its value from inside the cell $\triangle_0$, as the vector $(f'(u), g'(u))^T$ and take u as the indicator variable for the scalar case. For the Euler systems (2.11), v, again taking its value from inside the cell $\triangle_0$, is $(\mu, \nu)^T$ where μ is the velocity in the x-direction and ν is the velocity in the y-direction, and we take both the density ρ and the total energy E as the indicator variables. The target cell $\triangle_0$ is identified as a troubled cell when

$$\frac{|\int_{\partial\triangle_0^-}(u^h(x,y,t)|_{\triangle_0} - u^h(x,y,t)|_{\triangle_l})ds|}{h^{\frac{k+1}{2}}|\partial\triangle_0^-| \cdot ||u^h(x,y,t)|_{\triangle_0}||} > C_k, \tag{2.6}$$

where C_k is a constant, usually, we take $C_k = 1$ as in [15]. Here we choose h as the radius of the circumscribed circle in $\triangle_0$, and $\triangle_l, l = 1, 2, 3$, denote the neighboring cells sharing the edge(s) in $\partial\triangle_0^-$. u^h is the numerical solution corresponding to the indicator variable(s) and $||u^h(x,y,t)|_{\triangle_0}||$ is the standard L^2 norm in the cell $\triangle_0$.

2.3 The WENO limiting procedure for the scalar case on unstructured meshes

In this subsection, we present the details of the WENO limiting procedure for the scalar case.

Consider equation (1.1). In order to achieve better non-oscillatory qualities, the WENO reconstruction limiter is used. For a troubled cell $\triangle_0$, we reconstruct the polynomial $p_0(x, y)$ while retaining its cell average $u_0^{(0)}(t)$. We summarize the procedure to reconstruct the polynomial in the troubled cell $\triangle_0$ using the WENO reconstruction procedure.

Step 1.1. We select the WENO reconstruction stencil as $S = \{\triangle_0, \triangle_1, \triangle_2, \triangle_3\}$. Then we use the solutions of the DG method on such four cells and denote them as polynomials $p_0(x, y)$, $p_1(x, y)$, $p_2(x, y)$, $p_3(x, y)$, respectively. In order to maintain the original cell average

of $p_0(x,y)$ in the target cell $\triangle_0$, we modify the remaining three polynomials by

$$\tilde{p}_i(x,y) = p_i(x,y) - \frac{1}{|\triangle_0|}\int_{\triangle_0} p_i(x,y)dxdy + \frac{1}{|\triangle_0|}\int_{\triangle_0} p_0(x,y)dxdy, \quad i = 1,2,3.$$

For notational consistency we also denote $\tilde{p}_0(x,y) = p_0(x,y)$. The WENO reconstructed polynomial will be a convex combination of the four polynomials $\tilde{p}_i(x,y)$ with $i = 0,1,2,3$.

Step 1.2. We choose the linear weights denoted by $\gamma_0, ..., \gamma_3$. Notice that, since $\tilde{p}_i(x,y)$, for $i = 0,1,2,3$, are all $(k+1)$-th order approximations to the exact solution in smooth regions, there is no requirement on the values of these linear weights for accuracy besides $\gamma_0 + \gamma_1 + \gamma_2 + \gamma_3 = 1$. The choice of these linear weights is then solely based on the consideration of a balance between accuracy and ability to achieve essentially nonoscillatory shock transition. In all of our numerical tests, following the practice in [32, 9], we take $\gamma_0 = 0.997$ and $\gamma_1 = \gamma_2 = \gamma_3 = 0.001$.

Step 1.3. We compute the smoothness indicators, denoted by β_i, $i = 0, \ldots, 3$, which measure how smooth the functions $\tilde{p}_i(x,y)$, for $i = 0, \ldots, 3$, are on the target cell $\triangle_0$. The smaller these smoothness indicators, the smoother the functions are on the target cell. We use the same recipe for the smoothness indicators as in [14]:

$$\beta_i = \sum_{|\ell|=1}^{k} |\triangle_0|^{|\ell|-1} \int_{\triangle_0} \left(\frac{\partial^{|\ell|}}{\partial x^{\ell_1} \partial y^{\ell_2}} \tilde{p}_i(x,y) \right)^2 dxdy, \tag{2.7}$$

where $\ell = (\ell_1, \ell_2)$.

Step 1.4. We compute the non-linear weights based on the smoothness indicators:

$$\omega_i = \frac{\bar{\omega}_i}{\sum_{\ell=0}^{3} \bar{\omega}_\ell}, \qquad \bar{\omega}_\ell = \frac{\gamma_\ell}{(\varepsilon + \beta_\ell)^2}. \tag{2.8}$$

Here ε is a small positive number to avoid the denominator to become zero. We take $\varepsilon = 10^{-6}$ in our computation.

Step 1.5. The final nonlinear WENO reconstruction polynomial $p_0^{new}(x,y)$ is defined by a convex combination of the four (modified) polynomials in the stencil:

$$p_0^{new}(x,y) = \omega_0 \tilde{p}_0(x,y) + \omega_1 \tilde{p}_1(x,y) + \omega_2 \tilde{p}_2(x,y) + \omega_3 \tilde{p}_3(x,y). \tag{2.9}$$

It is easy to verify that $p_0^{new}(x,y)$ has the same cell average and order of accuracy as the original one $p_0(x,y)$ for the condition that $\sum_{i=0}^{3}\omega_i = 1$.

Step 1.6. The moments of the reconstructed polynomial are then given by:

$$u_0^{(l)}(t) = \frac{1}{\int_{\triangle_0}(v_l^{(0)}(x,y))^2\,dxdy}\int_{\triangle_0} p_0^{new}(x,y)\,v_l^{(0)}(x,y)dxdy, \qquad l = 1,\ldots,K. \tag{2.10}$$

We remark that, in Step 1.2 above, the choice of the linear weights is not unique. For accuracy, a larger value of γ_0 is better, since $\gamma_0 = 1$ corresponds to the unlimited case. However, a smaller value of γ_0 (hence a larger value of the other linear weights) would have a better chance for non-oscillatory performance of the algorithm. Our numerical experiments seem to indicate that the choice of values in Step 1.2 above is a good balance, but a variation around these values do not change the performance significantly.

For problems with non-periodic boundary conditions, we construct ghost cells according to the physical boundary conditions (e.g. reflective) to perform the limiter for the the boundary cells. Since our limiter uses only the immediate neighbors, this is not a significant burden to the algorithm near the boundary.

2.4 The WENO limiting procedure for the system case on unstructured meshes

In this subsection, we present the details of the WENO limiting procedure for systems.

Consider equation (1.1) where u, $f(u)$ and $g(u)$ are vectors with m components. In order to achieve better non-oscillatory qualities, the WENO reconstruction limiter is used with a local characteristic decomposition, see [26] for a discussion on the rationale in adopting such a decomposition. In this paper, we only consider the following Euler systems and set $m = 4$.

$$\begin{cases} u_t + f(u)_x + g(u)_y = \frac{\partial}{\partial t}\begin{pmatrix}\rho\\ \rho\mu\\ \rho\nu\\ E\end{pmatrix} + \frac{\partial}{\partial x}\begin{pmatrix}\rho\mu\\ \rho\mu^2+p\\ \rho\mu\nu\\ \mu(E+p)\end{pmatrix} + \frac{\partial}{\partial y}\begin{pmatrix}\rho\nu\\ \rho\mu\nu\\ \rho\nu^2+p\\ \nu(E+p)\end{pmatrix} = 0, \\ u(x,y,0) = u_0(x,y). \end{cases} \tag{2.11}$$

where ρ is the density, μ is the x-direction velocity, ν is the y-direction velocity, E is the total energy, $p = \frac{E}{\gamma-1} - \frac{1}{2}\rho(\mu^2+\nu^2)$ is the pressure and $\gamma = 1.4$ in our test cases. We denote the Jacobian matrices as $(f'(u), g'(u)) \cdot n_i$ and $n_i = (n_{ix}, n_{iy})^T, i = 1, 2, 3$, are the outward unit normals to different edges of the target cell. We then give the left and right eigenvectors of such Jacobian matrices as:

$$L_i = \begin{pmatrix} \frac{B_2+(\mu n_{ix}+\nu n_{iy})/c}{2} & -\frac{B_1\mu+n_{ix}/c}{2} & -\frac{B_1\nu+n_{iy}/c}{2} & \frac{B_1}{2} \\ n_{iy}\mu - n_{ix}\nu & -n_{iy} & n_{ix} & 0 \\ 1-B_2 & B_1\mu & B_1\nu & -B_1 \\ \frac{B_2-(\mu n_{ix}+\nu n_{iy})/c}{2} & -\frac{B_1\mu-n_{ix}/c}{2} & -\frac{B_1\nu-n_{iy}/c}{2} & \frac{B_1}{2} \end{pmatrix}, \tag{2.12}$$

and

$$R_i = \begin{pmatrix} 1 & 0 & 1 & 1 \\ \mu - cn_{ix} & -n_{iy} & \mu & \mu + cn_{ix} \\ \nu - cn_{iy} & n_{ix} & \nu & \nu + cn_{iy} \\ H - c(\mu n_{ix} + \nu n_{iy}) & -n_{iy}\mu + n_{ix}\nu & \frac{\mu^2+\nu^2}{2} & H + c(\mu n_{ix} + \nu n_{iy}) \end{pmatrix}, i = 1, 2, 3, \tag{2.13}$$

where $c = \sqrt{\gamma p/\rho}$, $B_1 = (\gamma-1)/c^2$, $B_2 = B_1(\mu^2+\nu^2)/2$ and $H = (E+p)/\rho$. If the troubled cell $\triangle_0$ is detected by the KXRCF technique [15] using (2.6), we denote as before the four modified polynomial vectors $\tilde{p}_0$, $\tilde{p}_1$, $\tilde{p}_2$, $\tilde{p}_3$, corresponding to the cell $\triangle_0$ and its three immediate neighbors and having the same cell average as p_0 on $\triangle_0$. We then perform the WENO limiting procedure as follows:

Step 2.1. In each n_i-direction among the three normal directions of the three edges of the cell $\triangle_0$, we reconstruct a new polynomial vector $(p_0)_i^{new}$ by using the characteristic-wise WENO limiting procedure with the associated Jacobian $f'(u)n_{ix} + g'(u)n_{iy}$:

– Step 2.1.1. Project the polynomial vectors $\tilde{p}_0$, $\tilde{p}_1$, $\tilde{p}_2$ and $\tilde{p}_3$ into the characteristic fields $\bar{p}_l = L_i \cdot \tilde{p}_l$, $l = 0, 1, 2, 3$, each of them being a 4-component vector and each component of the vector is a k-th degree polynomial.

– Step 2.1.2. Perform Step 1.1 to Step 1.5 of the WENO limiting procedure that has been specified for the scalar case, to obtain a new 4-component vector on the troubled cell $\triangle_0$ as $\bar{p}_0^{new}$.

– Step 2.1.3. Project $\bar{p}_0^{new}$ into the physical space $(p_0)_i^{new} = R_i \cdot \bar{p}_0^{new}$.

Step 2.2. The final new 4-component vector on the troubled cell $\triangle_0$ is defined as $p_0^{new} = \frac{\sum_{i=1}^{3}(p_0)_i^{new}|\triangle_i|}{\sum_{i=1}^{3}|\triangle_i|}$.

Step 2.3. The moments of the reconstructed polynomials which are components of the vector on $\triangle_0$ are then computed similarly as in Step 1.6..

3 Numerical results

In this section, we provide numerical results to demonstrate the performance of the WENO reconstruction limiters for the RKDG methods on unstructured meshes described in Section 2.

We first test the accuracy of the schemes in two dimensional problems. In all of our accuracy test cases, the refinement is performed by a structured refinement (we simply break each triangle into four similar smaller triangles for each level of the refinement). We adjust the constant C_k in (2.6) from 1 to 0.01 in Example 3.1, to 0.01 (for the second order RKDG method) and 0.001 (for the third order RKDG method) in Example 3.2, and to 0.001 for Example 3.3, for the purpose of artificially generating a larger percentage of troubled cells in order to test accuracy when the WENO reconstruction procedure is enacted in more cells. We also consider the case of artificially declare all cells to be troubled cells for Example 3.3 in order to assess the effect of the WENO limiter on accuracy in such situation. The CFL number is set to be 0.3 for the second order ($k = 1$) and 0.18 for the third order ($k = 2$) RKDG methods.

Example 3.1. We solve the following nonlinear scalar Burgers equation in two dimensions:

$$u_t + \left(\frac{u^2}{2}\right)_x + \left(\frac{u^2}{2}\right)_y = 0 \tag{3.1}$$

with the initial condition $u(x, y, 0) = 0.5 + \sin(\pi(x + y)/2)$ and periodic boundary conditions in both directions. We compute the solution up to $t = 0.5/\pi$, when the solution is still smooth. For this test case the coarsest mesh we have used is shown in Figure 3.1. The errors and numerical orders of accuracy for the RKDG method with the WENO limiter comparing

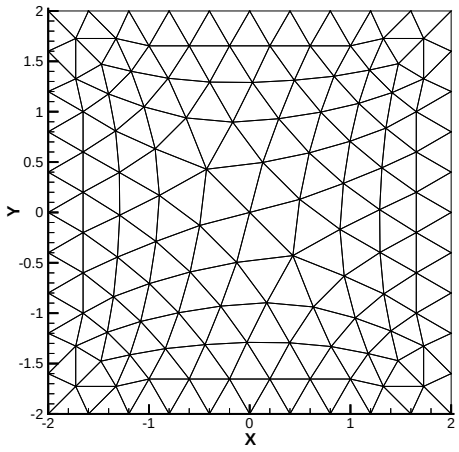

Figure 3.1: Burgers equation. The coarsest mesh. The mesh points on the boundary are uniformly distributed with cell length $h = 4/10$.

with the original RKDG method without limiter are shown in Table 3.1. In Table 3.2, we document the percentage of cells declared to be troubled cells for different mesh levels and orders of accuracy. We can see that the WENO limiter keeps the designed order of accuracy, even when a large percentage of good cells are artificially identified as troubled cells.

Example 3.2. We solve the Euler equations (2.11). The initial conditions are: $\rho(x, y, 0) = 1 + 0.2\sin(\pi(x + y))$, $\mu(x, y, 0) = 0.7$, $\nu(x, y, 0) = 0.3$, $p(x, y, 0) = 1$. Periodic boundary conditions are applied in both directions. The exact solution is $\rho(x, y, t) = 1 + 0.2\sin(\pi(x + y - t))$. We compute the solution up to $t = 2$. For this test case the coarsest mesh we have used is shown in Figure 3.2. The errors and numerical orders of accuracy of the density for the RKDG method with the WENO limiter comparing with the original RKDG method without a limiter are shown in Table 3.3. In Table 3.4, we document the percentage of cells declared to be troubled cells for different mesh levels and orders of accuracy. Similar to the previous example, we can see that the WENO limiter again keeps the designed order of accuracy when the mesh size is small enough, even when a large percentage of good cells are artificially identified as troubled cells.

Example 3.3. In order to check accuracy and convergence properties of the RKDG method

Table 3.1: $u_t + \left(\frac{u^2}{2}\right)_x + \left(\frac{u^2}{2}\right)_y = 0$. $u(x, y, 0) = 0.5 + \sin(\pi(x + y)/2)$. Periodic boundary conditions in both directions. $T = 0.5/\pi$. L^1 and L^∞ errors. RKDG with the WENO limiter compared to RKDG without limiter.

		DG with WENO limiter				DG without limiter			
	cell length h	L^1 error	order	L^∞ error	order	L^1 error	order	L^∞ error	order
P^1	4/10	7.47E-2		7.33E-1		2.41E-2		2.56E-1	
	4/20	1.58E-2	2.24	2.94E-1	1.32	6.07E-3	1.99	7.54E-2	1.77
	4/40	2.39E-3	2.73	4.04E-2	2.86	1.53E-3	1.98	2.14E-2	1.81
	4/80	4.27E-4	2.48	5.68E-3	2.83	3.91E-4	1.97	5.71E-3	1.91
	4/160	9.88E-5	2.11	1.55E-3	1.87	9.87E-5	1.99	1.55E-3	1.88
P^2	4/10	1.61E-3		5.32E-2		1.70E-3		5.28E-2	
	4/20	2.30E-4	2.81	8.12E-3	2.71	2.45E-4	2.79	8.19E-3	2.69
	4/40	3.27E-5	2.81	1.55E-3	2.38	3.17E-5	2.95	1.55E-3	2.39
	4/80	4.64E-6	2.82	2.91E-4	2.42	4.01E-6	2.98	2.37E-4	2.71
	4/160	5.68E-7	3.03	4.28E-5	2.76	5.03E-7	3.00	3.20E-5	2.89

Table 3.2: $u_t + \left(\frac{u^2}{2}\right)_x + \left(\frac{u^2}{2}\right)_y = 0$. $u(x, y, 0) = 0.5 + \sin(\pi(x + y)/2)$. Periodic boundary conditions in both directions. $T = 0.5/\pi$. The average percentage of troubled cells subject to the WENO limiting for different meshes.

Percentage of the troubled cells					
	cell length h	average percentage		cell length h	average percentage
P^1	4/10	92.4	P^2	4/10	65.7
	4/20	81.3		4/20	35.9
	4/40	69.2		4/40	17.3
	4/80	54.3		4/80	7.58
	4/160	37.3		4/160	1.81

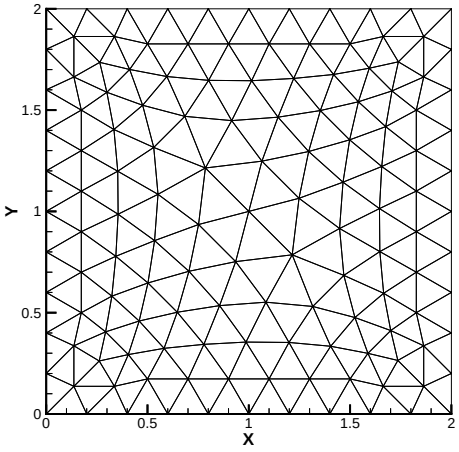

Figure 3.2: 2D-Euler equations. Mesh. The mesh points on the boundary are uniformly distributed with cell length $h = 2/10$.

Table 3.3: 2D-Euler equations: initial data $\rho(x, y, 0) = 1 + 0.2\sin(\pi(x + y))$, $u(x, y, 0) = 0.7$, $v(x, y, 0) = 0.3$, and $p(x, y, 0) = 1$. Periodic boundary conditions in both directions. $T = 2.0$. L^1 and L^∞ errors. RKDG with the WENO limiter compared to RKDG without limiter.

		DG with WENO limiter				DG without limiter			
	cell length h	L^1 error	order	L^∞ error	order	L^1 error	order	L^∞ error	order
P^1	2/10	3.57E-2		8.94E-2		4.39E-3		2.23E-2	
	2/20	5.67E-3	2.65	2.59E-2	1.78	1.03E-3	2.08	5.42E-3	2.04
	2/40	6.28E-4	3.17	4.54E-3	2.51	2.54E-4	2.02	1.29E-3	2.06
	2/80	6.40E-5	3.29	3.80E-4	3.58	6.38E-5	1.99	3.27E-4	1.98
	2/160	1.62E-5	1.98	8.48E-5	2.16	1.62E-5	1.97	8.48E-5	1.95
P^2	2/10	6.04E-4		5.79E-3		4.48E-4		5.94E-3	
	2/20	9.00E-5	2.75	1.14E-3	2.34	6.17E-5	2.86	1.14E-3	2.38
	2/40	1.01E-5	3.14	1.59E-4	2.84	7.05E-6	3.12	1.94E-4	2.56
	2/80	7.99E-7	3.67	2.77E-5	2.53	7.76E-7	3.18	2.87E-5	2.76
	2/160	1.10E-7	2.86	3.62E-6	2.93	1.10E-7	2.81	3.62E-6	2.99

Table 3.4: 2D-Euler equations: initial data $\rho(x, y, 0) = 1 + 0.2\sin(\pi(x + y))$, $u(x, y, 0) = 0.7$, $v(x, y, 0) = 0.3$, and $p(x, y, 0) = 1$. Periodic boundary conditions in both directions. $T = 2.0$. The average percentage of troubled cells subject to the WENO limiting for different meshes.

Percentage of the troubled cells					
	cell length h	average percentage		cell length h	average percentage
P^1	2/10	65.7	P^2	2/10	81.1
	2/20	32.3		2/20	53.5
	2/40	11.6		2/40	25.9
	2/80	1.42E-2		2/80	6.91E-2
	2/160	2.11E-4		2/160	5.31E-4

with the WENO limiters for problems with curved boundary, we solve the subsonic flow past a circular cylinder at a Mach number of $M_\infty = 0.38$ [18]. The four refined triangular meshes (again with structured refinement) are used here and the associated meshes are shown in Figure 3.3. The radius of the cylinder is 0.5, and the computational domain is $\{(x, y) : 0.5 \leq |\sqrt{x^2 + y^2} \leq 20\}$. The numbers of points in the inner and outer boundaries are the same as 16, 32, 64 and 128, respectively. RKDG method with and without WENO limiters, with curved boundary conditions, and with k=1 and k=2 (second and third order), are used in the numerical experiments. Mach number contours are shown in Figure 3.4 and Figure 3.5. Following [18], we measure the entropy error by the formula

$$\frac{S_0 - S_\infty}{S_\infty} = \frac{\frac{p_0}{{\rho_0}^\gamma}}{\frac{p_\infty}{{\rho_\infty}^\gamma}} - 1$$

where S_0 is the local entropy and S_∞ is the far field entropy. The L^2 errors and numerical orders of accuracy for the entropy for the RKDG method with WENO limiters on every cell, with WENO limiters only on the troubled cells and without the WENO limiters are shown in Table 3.5. We can see that the new WENO limiter can maintain the designed high order accuracy of the DG method, even in the extreme situation that WENO limiter is applied on every cell.

We now test the performance of the RKDG method with the WENO limiters for problems containing shocks. From now on, we reset the constant $C_k = 1$ in the trouble cell indicator

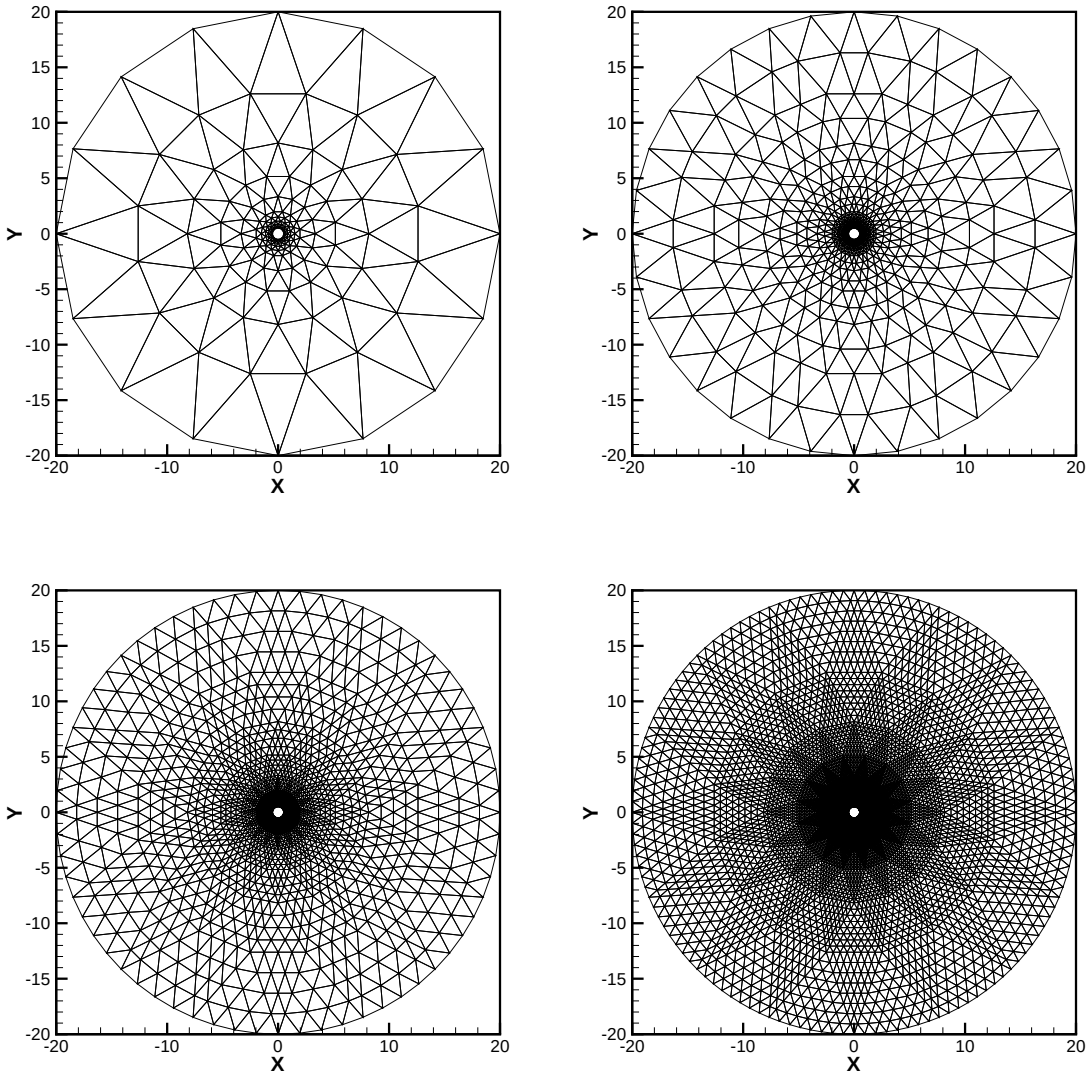

Figure 3.3: Subsonic cylinder test case. Sample meshes. From left to right and top to bottom: the numbers of points in the inner and outer boundaries are the same as 16, 32, 64 and 128.

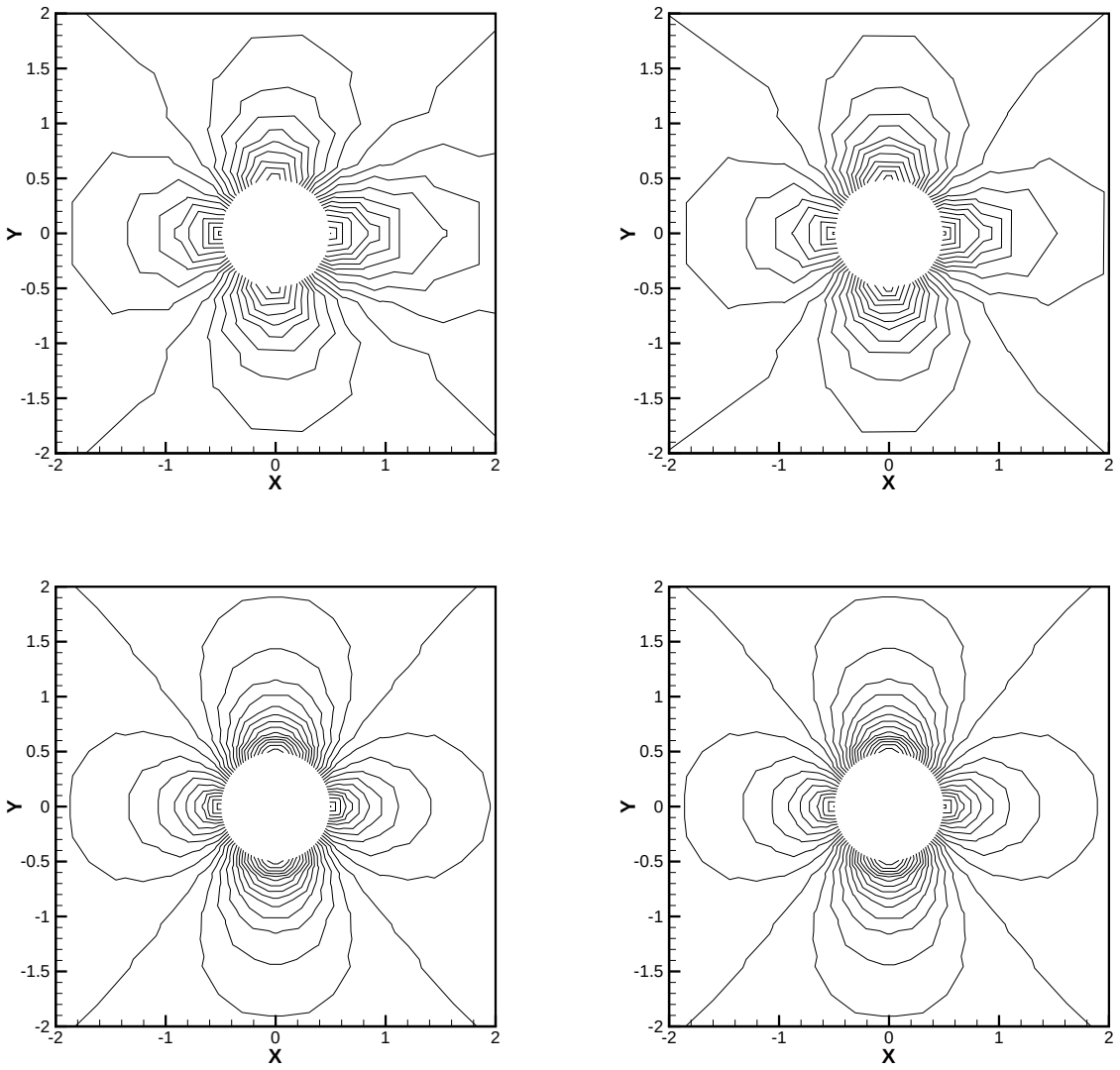

Figure 3.4: Subsonic cylinder test case. RKDG with WENO limiter. Zoom-in pictures around the cylinder. 30 equally spaced Mach number contours from 0.04 to 0.94. Left: second order ($k = 1$); right: third order ($k = 2$). From top to bottom: the numbers of points in the inner and outer boundaries are the same as 16 and 32.

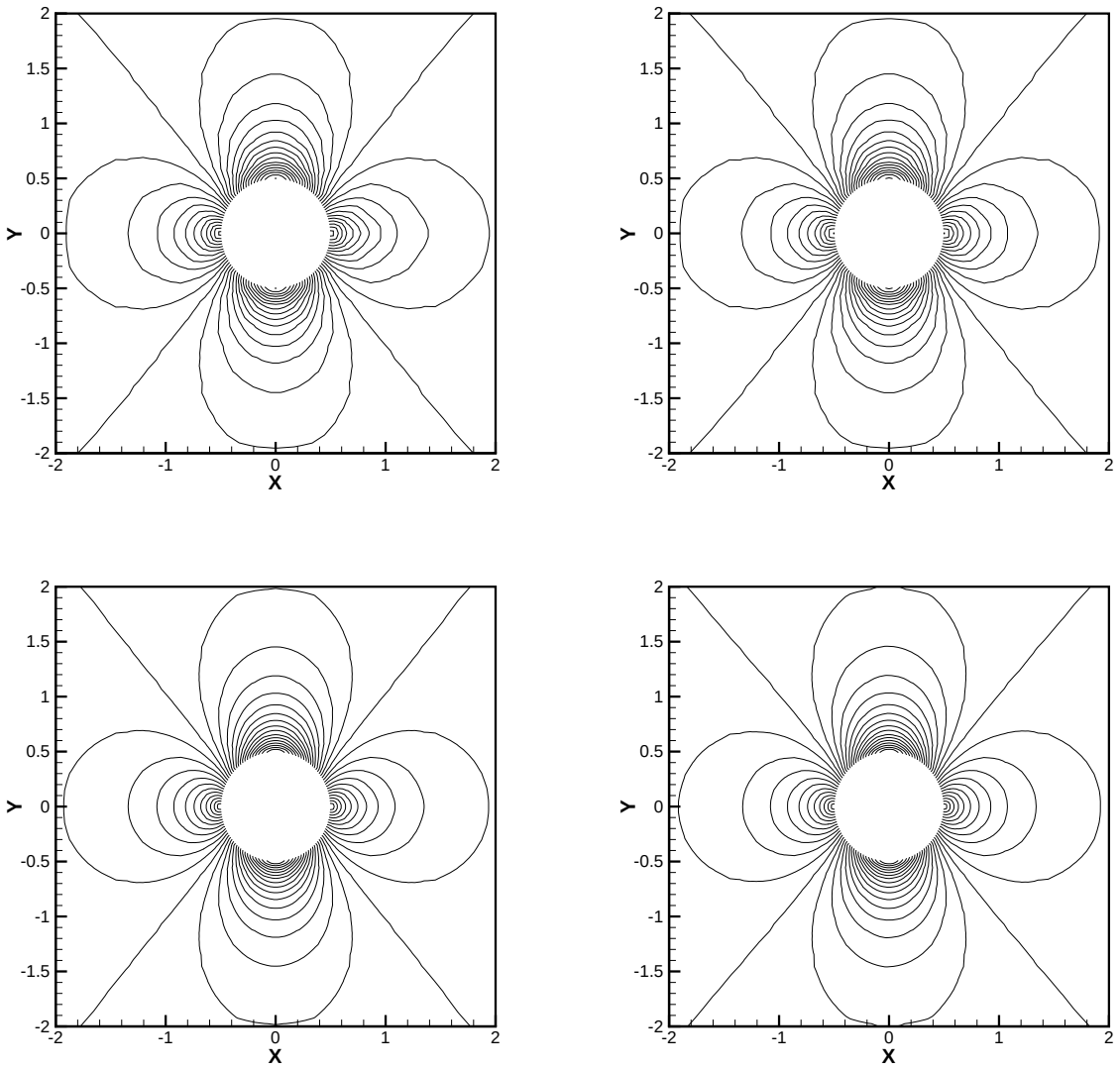

Figure 3.5: Subsonic cylinder test case. RKDG with WENO limiter. Zoom-in pictures around the cylinder. 30 equally spaced Mach number contours from 0.04 to 0.94. Left: second order ($k = 1$); right: third order ($k = 2$). From top to bottom: the numbers of points in the inner and outer boundaries are the same as 64 and 128.

Table 3.5: Subsonic cylinder test case. L^2 entropy errors and orders of convergence. RKDG with the WENO limiter compared to RKDG without limiter.

	DG with WENO limiter on every cell				DG with WENO limiter, $C_k = 0.001$			
	P^1		P^2		P^1		P^2	
cell number	L^2 error	order	L^2 error	order	L^2 error	order	L^2 error	order
320	1.09E-2		5.11E-3		4.61E-3		1.87E-3	
1280	1.55E-3	2.80	4.22E-4	3.59	7.76E-4	2.57	2.01E-4	3.22
5120	3.14E-4	2.30	4.57E-5	3.20	1.24E-4	2.64	2.12E-5	3.25
20480	6.42E-5	2.29	5.20E-6	3.13	2.16E-5	2.52	2.34E-6	3.18
	DG without limiter							
	P^1				P^2			
cell number	L^2 error		order		L^2 error		order	
320	4.59E-3				1.81E-3			
1280	7.70E-4		2.56		1.99E-4		3.18	
5120	1.10E-4		2.80		2.08E-5		3.25	
20480	2.11E-5		2.38		2.22E-6		3.22	

(2.6). For comparison with the RKDG method using the *minmod* TVB limiter, we refer to the results in [4, 7]. For comparison with the RKDG method using the previous versions of WENO type limiters, we refer to the results in [18, 34].

Example 3.4. We solve the same nonlinear Burgers equation (3.1) with the same initial condition $u(x, y, 0) = 0.5 + \sin(\pi(x + y)/2)$, except that we plot the results at $t = 1.5/\pi$ when a shock has already appeared in the solution. The solutions are shown in Figure 3.6. We can see that the schemes give non-oscillatory shock transitions for this problem.

Example 3.5. Double Mach reflection problem. This model problem is originally from [30]. We solve the Euler equations (2.11) in a computational domain of $[0, 4] \times [0, 1]$. The reflection boundary condition is used at the wall, which for the rest of the bottom boundary (the part from $x = 0$ to $x = \frac{1}{6}$), the exact post-shock condition is imposed. At the top boundary is the exact motion of the Mach 10 shock. The results shown are at $t = 0.2$. Two different orders of accuracy for the RKDG with WENO limiters, k=1 and k=2 (second and third order), are used in the numerical experiments. A sample mesh coarser than what is

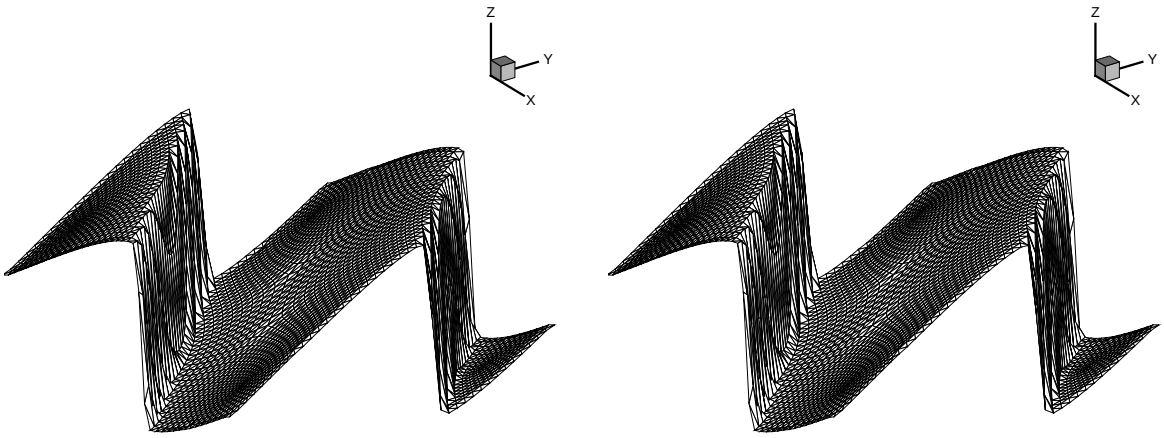

Figure 3.6: Burgers equation. $T = 1.5/\pi$. The surface of the solution. The mesh points on the boundary are uniformly distributed with cell length $h = 4/40$. RKDG with the WENO limiter. Left: second order ($k = 1$); right: third order ($k = 2$).

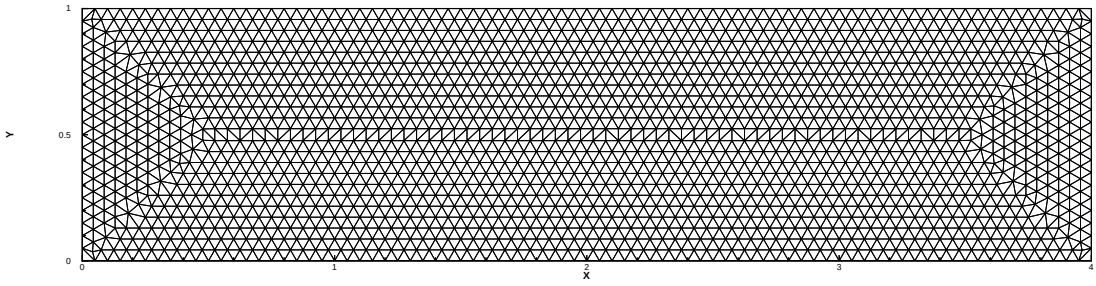

Figure 3.7: Double Mach refection problem. Sample mesh. The mesh points on the boundary are uniformly distributed with cell length $h = 1/20$.

used is shown in Figure 3.7. In Table 3.6 we document the percentage of cells declared to be troubled cells for different orders of accuracy. We can see that only a small percentage of cells are declared as troubled cells. The simulation results are shown in Figures 3.8 and 3.9. The "zoomed-in" pictures around the double Mach stem to show more details are given in Figure 3.10. The troubled cells identified at the last time step are shown in Figures 3.11 and 3.12. Clearly, the resolution improves with an increasing k on the same mesh.

Example 3.6. A Mach 3 wind tunnel with a step. This model problem is also originally from [30]. The setup of the problem is as follows. The wind tunnel is 1 length unit wide and

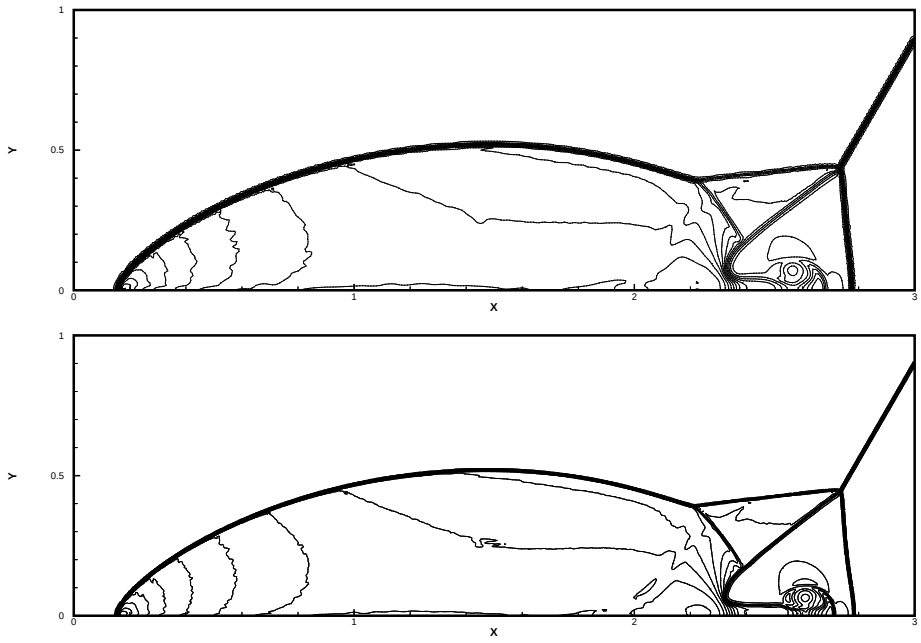

Figure 3.8: Double Mach refection problem. Second order ($k = 1$) RKDG with the WENO limiter. 30 equally spaced density contours from 1.1 to 22. Top: the mesh points on the boundary are uniformly distributed with cell length $h = 1/100$; bottom: $h = 1/200$.

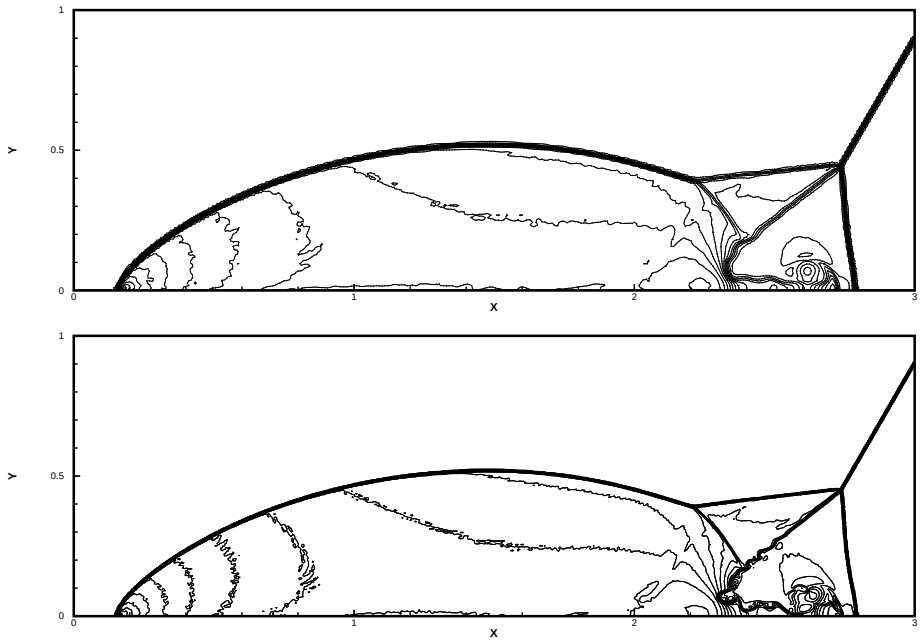

Figure 3.9: Double Mach refection problem. Third order ($k = 2$) RKDG with the WENO limiter. 30 equally spaced density contours from 1.1 to 22. Top: the mesh points on the boundary are uniformly distributed with cell length $h = 1/100$; bottom: $h = 1/200$.

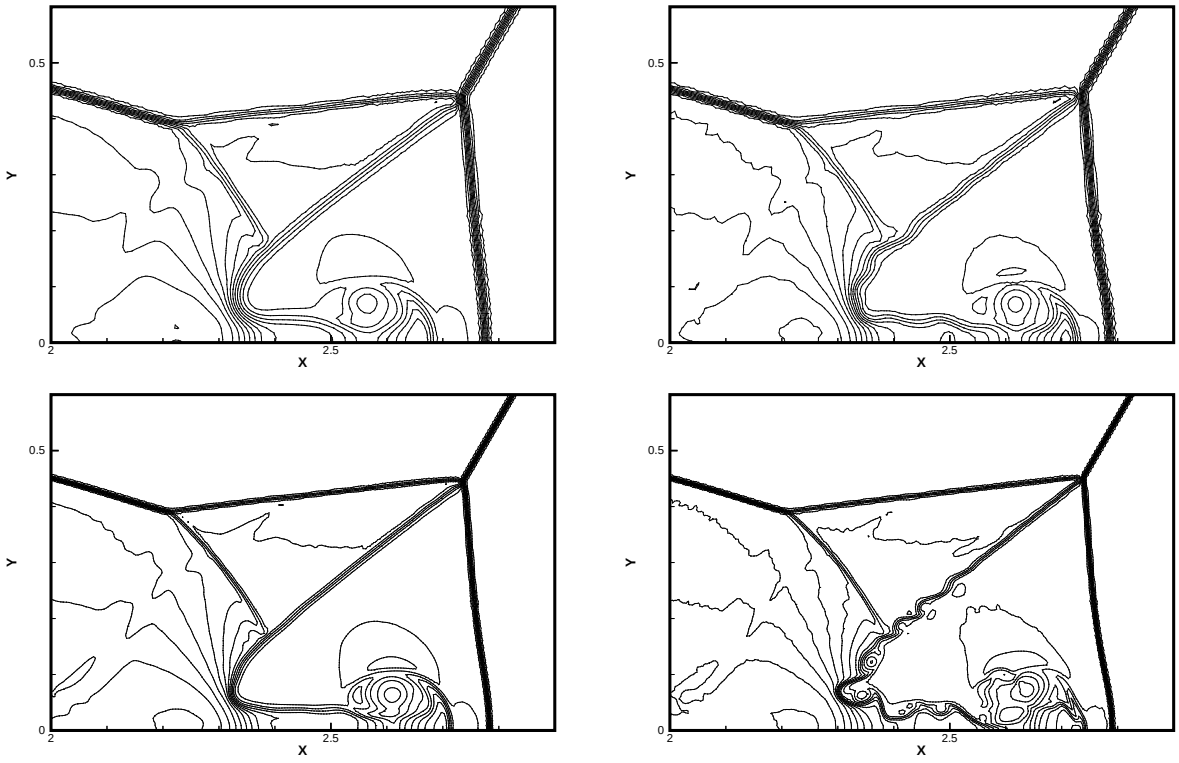

Figure 3.10: Double Mach refection problem. RKDG with the WENO limiter. Zoom-in pictures around the Mach stem. 30 equally spaced density contours from 1.1 to 22. Left: second order ($k = 1$); right: third order ($k = 2$). Top: the mesh points on the boundary are uniformly distributed with cell length $h = 1/100$; bottom: $h = 1/200$.

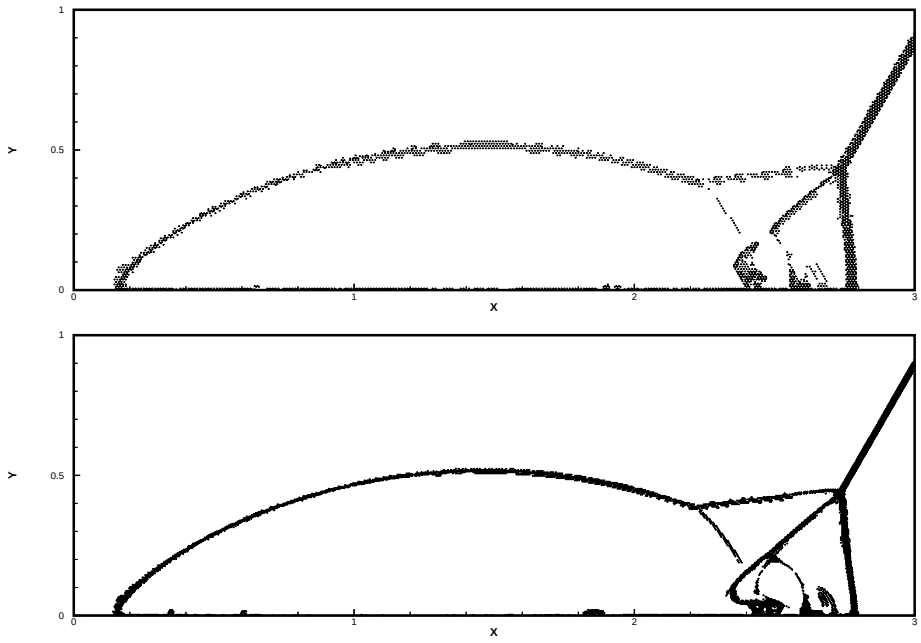

Figure 3.11: Double Mach refection problem. Second order ($k = 1$) RKDG with the WENO limiter. Troubled cells. Circles denote triangles which are identified as troubled cells subject to the WENO limiting. Top: the mesh points on the boundary are uniformly distributed with cell length $h = 1/100$; bottom: $h = 1/200$.

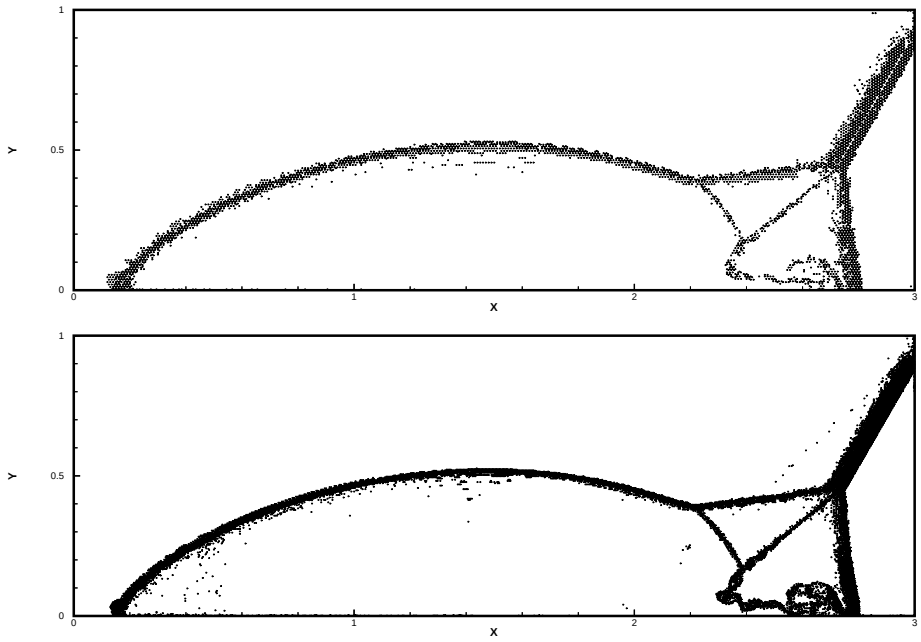

Figure 3.12: Double Mach refection problem. Third order ($k = 2$) RKDG with the WENO limiter. Troubled cells. Circles denote triangles which are identified as troubled cells subject to the WENO limiting. Top: the mesh points on the boundary are uniformly distributed with cell length $h = 1/100$; bottom: $h = 1/200$.

Table 3.6: Double Mach refection problem. The maximum and average percentages of troubled cells subject to the WENO limiting.

Percentage of the troubled cells							
P^1	cell length h	1/100	1/200	P^2	cell length h	1/100	1/200
	maximum percentage	3.61	2.34		maximum percentage	4.83	4.30
	average percentage	2.18	1.41		average percentage	3.00	2.59

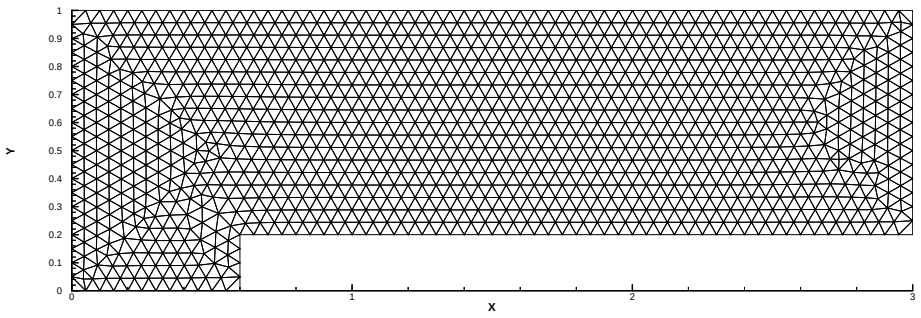

Figure 3.13: Forward step problem. Sample mesh. The mesh points on the boundary are uniformly distributed with cell length $h = 1/20$.

3 length units long. The step is 0.2 length units high and is located 0.6 length units from the left-hand end of the tunnel. The problem is initialized by a right-going Mach 3 flow. Reflective boundary conditions are applied along the wall of the tunnel and inflow/outflow boundary conditions are applied at the entrance/exit. At the corner of the step, there is a singularity. However we do not modify our schemes or refine the mesh near the corner, in order to test the performance of our schemes for such singularity. The results are shown at $t = 4$. We present a sample triangulation of the whole region $[0, 3] \times [0, 1]$ in Figure 3.13. In Table 3.7 we document the percentage of cells declared to be troubled cells for different orders of accuracy. In Figure 3.14, we show 30 equally spaced density contours from 0.32 to 6.15 computed by the second and third order RKDG schemes with the WENO limiters, respectively. The troubled cells identified at the last time step are shown in Figure 3.15. We can clearly observe that the third order scheme gives better resolution than the second order scheme, especially for the resolution of the physical instability and roll-up of the contact line.

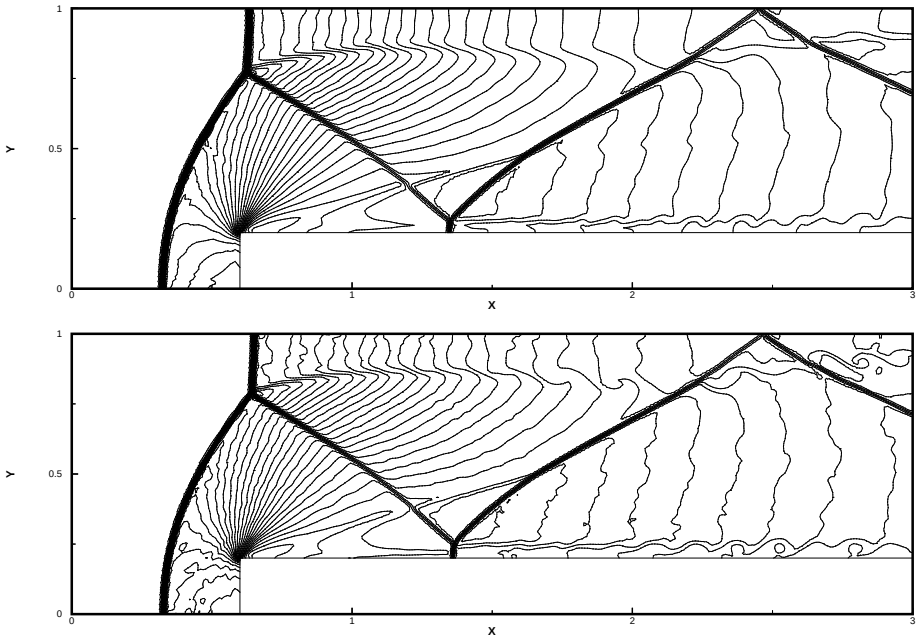

Figure 3.14: Forward step problem. Top: second order ($k = 1$); bottom: third order ($k = 2$) RKDG with the WENO limiter. 30 equally spaced density contours from 0.32 to 6.15. The mesh points on the boundary are uniformly distributed with cell length $h = 1/100$.

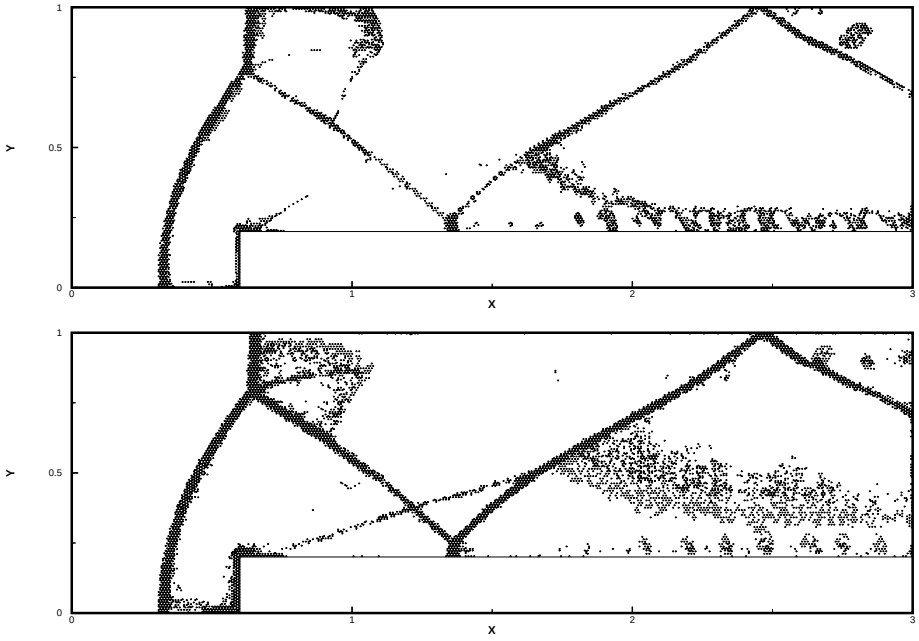

Figure 3.15: Forward step problem. Top: second order ($k = 1$); bottom: third order ($k = 2$) RKDG with the WENO limiter. Troubled cells. Circles denote triangles which are identified as troubled cell subject to the WENO limiting. The mesh points on the boundary are uniformly distributed with cell length $h = 1/100$.

Table 3.7: Forward step problem. The maximum and average percentages of troubled cells subject to the WENO limiting.

Percentage of the troubled cells							
P^1	cell length h	1/60	1/100	P^2	cell length h	1/60	1/100
	maximum percentage	7.08	5.49		maximum percentage	8.44	8.11
	average percentage	5.33	3.70		average percentage	5.80	5.44

Example 3.7. We consider inviscid Euler transonic flow past a single NACA0012 airfoil configuration with Mach number $M_\infty = 0.8$, angle of attack $\alpha = 1.25^\circ$ and with $M_\infty = 0.85$, angle of attack $\alpha = 1^\circ$. The computational domain is $[-15, 15] \times [-15, 15]$. The mesh used in the computation is shown in Figure 3.16, consisting of 9340 elements with the maximum diameter of the circumcircle being 1.4188 and the minimum diameter being 0.0031 near the airfoil. The mesh uses curved cells near the airfoil. The second order RKDG scheme with the WENO limiter and the third order scheme with the WENO limiter are used in the numerical experiments. In Table 3.8, we document the percentage of cells declared to be troubled cells for different orders of accuracy. Mach number and pressure distributions are shown in Figures 3.17 and 3.18. We can see that the third order scheme has better resolution than the second order one. The troubled cells identified at the last time step are shown in Figure 3.19. Clearly, very few cells are identified as troubled cells.

Table 3.8: NACA0012 airfoil problem. The maximum and average percentages of troubled cells subject to the WENO limiting.

	$M_\infty = 0.8$, angle of attack $\alpha = 1.25^\circ$		$M_\infty = 0.85$, angle of attack $\alpha = 1^\circ$	
P^1	maximum percentage	11.3	maximum percentage	11.6
	average percentage	6.49	average percentage	6.72
P^2	maximum percentage	18.1	maximum percentage	18.7
	average percentage	10.4	average percentage	12.8

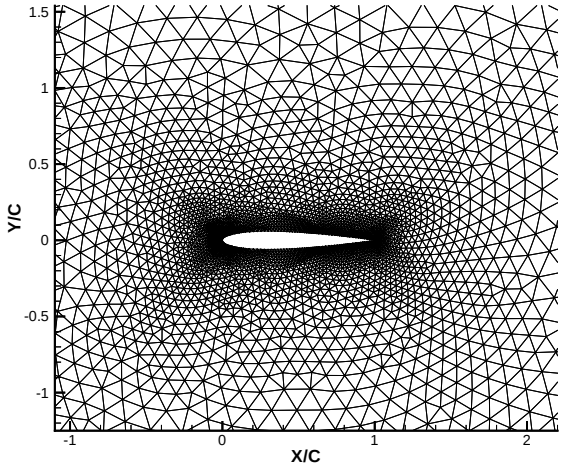

Figure 3.16: NACA0012 airfoil mesh zoom in.

4 Concluding remarks

We have generalized the simple weighted essentially non-oscillatory (WENO) limiter, originally developed in [32] for structured meshes, to two-dimensional unstructured triangular meshes for the Runge-Kutta discontinuous Galerkin (RKDG) methods solving hyperbolic conservation laws. The general framework of WENO limiters for RKDG methods, namely first identifying troubled cells subject to the WENO limiting (in this paper we use the KXRCF technique [15] for this purpose), then reconstructing the polynomial solution inside the troubled cell by the solutions of the DG method on the target cell and its neighboring cells by a WENO procedure, is followed in this paper. The main novelty of this paper is the apparent simplicity of the WENO reconstruction procedure, which uses only the information from the troubled cell and its three immediate neighbors, without extensive usage of any geometric information of the meshes, and with simple positive linear weights in the reconstruction procedure. Extensive numerical results, both for scalar equations and for Euler systems of compressible gas dynamics, are provided to demonstrate good results, both in accuracy and in non-oscillatory performance, comparable with those in earlier literature with much more complicated WENO limiters. In future work, we will extend the methodology to three-dimensional unstructured meshes.

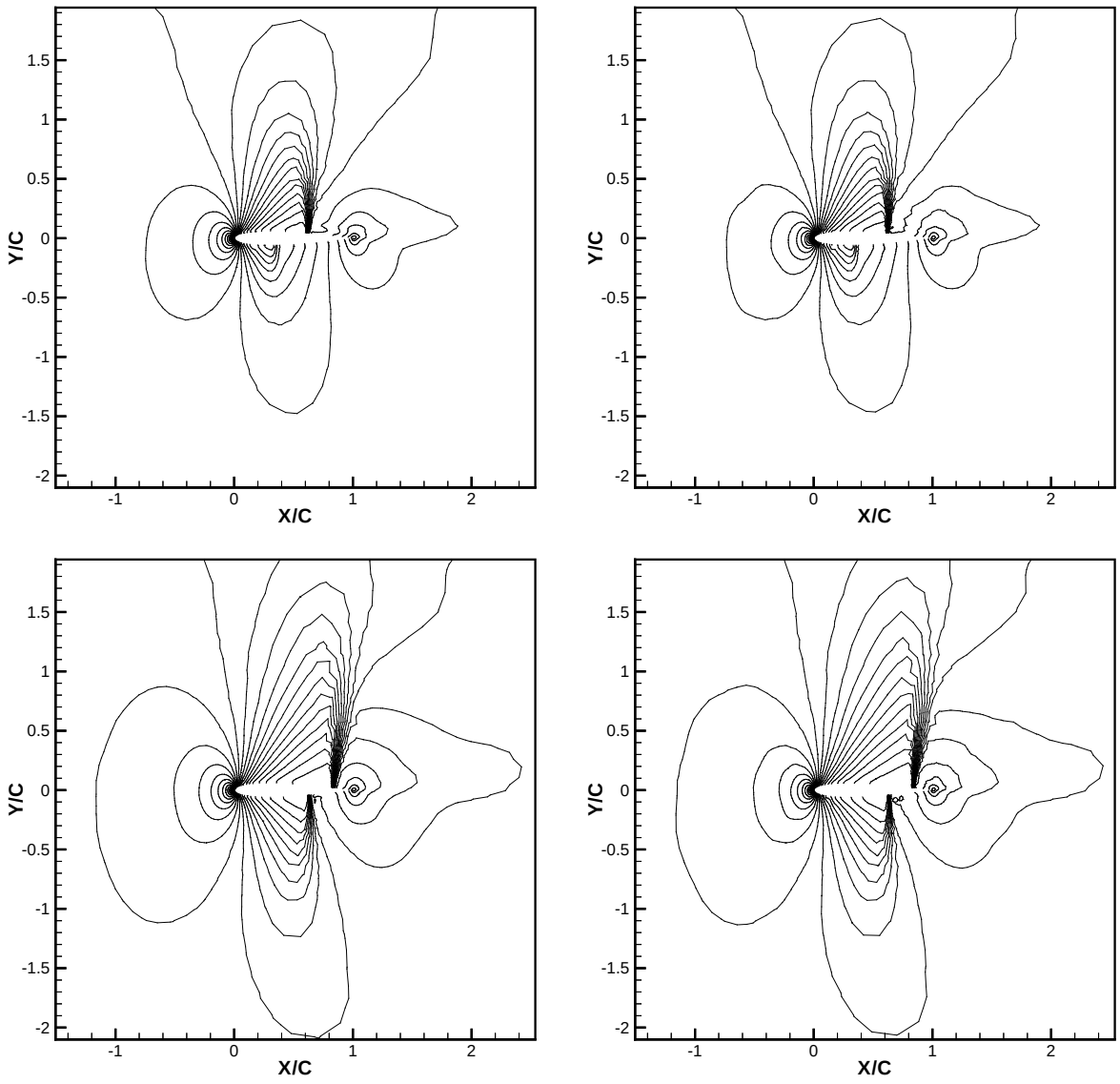

Figure 3.17: NACA0012 airfoil. Mach number. Top: $M_\infty = 0.8$, angle of attack $\alpha = 1.25°$, 30 equally spaced Mach number contours from 0.172 to 1.325; bottom: $M_\infty = 0.85$, angle of attack $\alpha = 1°$, 30 equally spaced Mach number contours from 0.158 to 1.357. Left: second order ($k = 1$); right: third order ($k = 2$) RKDG with the WENO limiter.

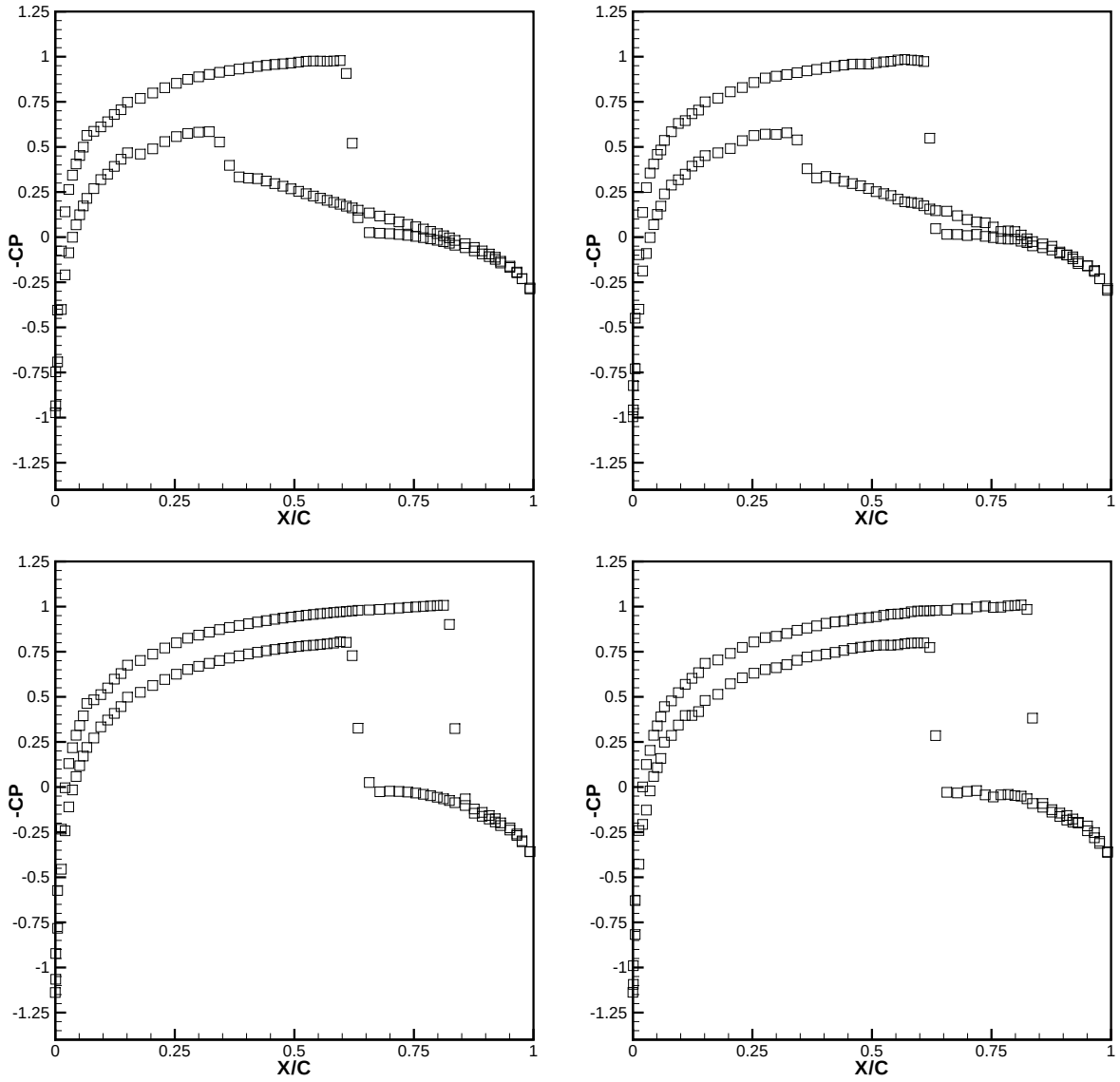

Figure 3.18: NACA0012 airfoil. Pressure distribution. Top: $M_\infty = 0.8$, angle of attack $\alpha = 1.25°$; bottom: $M_\infty = 0.85$, angle of attack $\alpha = 1°$. Left: second order ($k = 1$); right: third order ($k = 2$) RKDG with the WENO limiter.

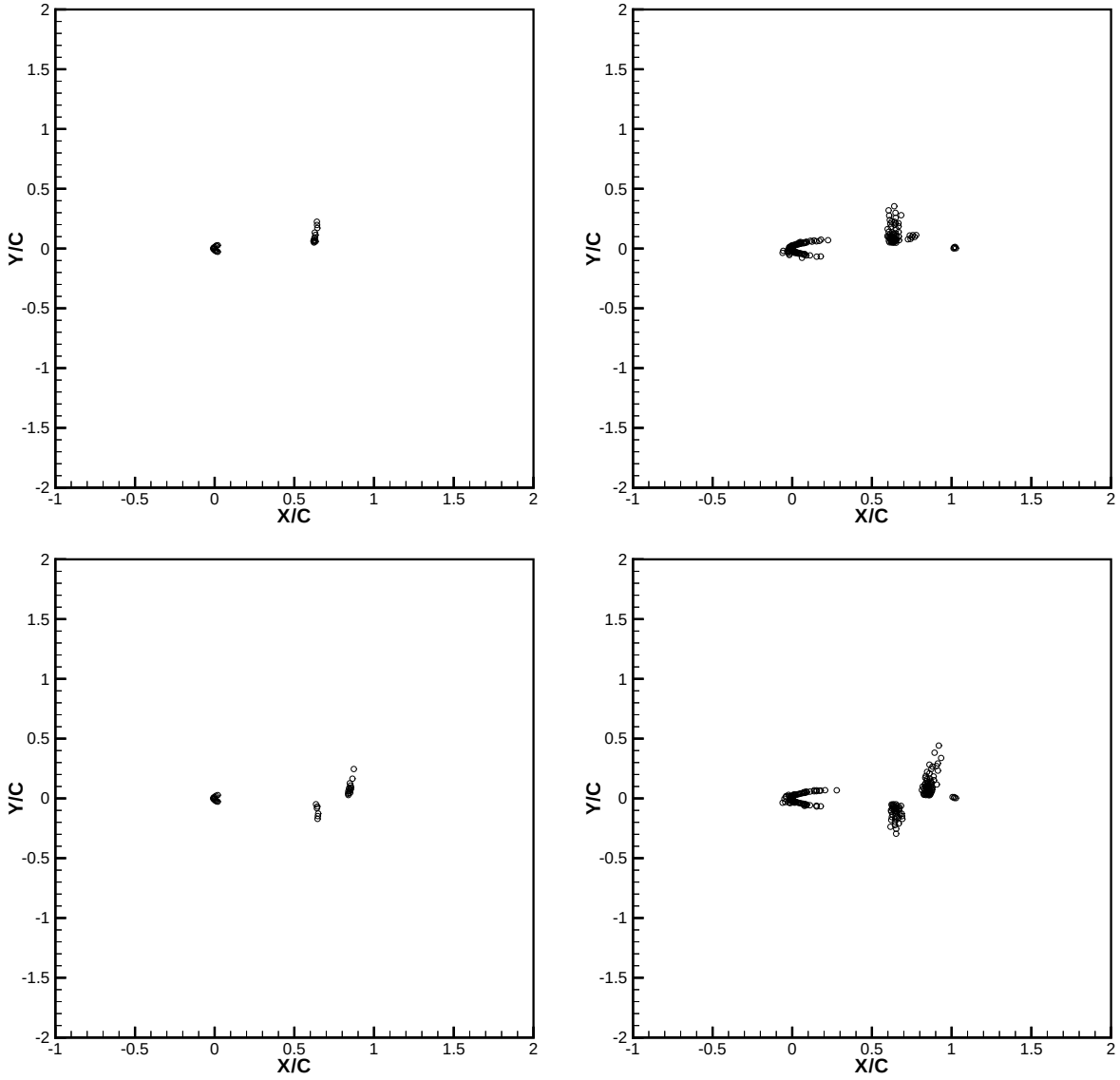

Figure 3.19: NACA0012 airfoil. Troubled cells. Circles denote triangles which are identified as troubled cells subject to the WENO limiting. Top: $M_\infty = 0.8$, angle of attack $\alpha = 1.25°$; bottom: $M_\infty = 0.85$, angle of attack $\alpha = 1°$. Left: second order ($k = 1$); right: third order ($k = 2$) RKDG with the WENO limiter.

References

[1] R. Biswas, K.D. Devine and J. Flaherty, *Parallel, adaptive finite element methods for conservation laws*, Applied Numerical Mathematics, 14 (1994), 255-283.

[2] A. Burbeau, P. Sagaut and C.H. Bruneau, *A problem-independent limiter for high-order Runge-Kutta discontinuous Galerkin methods*, Journal of Computational Physics, 169 (2001), 111-150.

[3] B. Cockburn, *Discontinuous Galerkin methods for convection-dominated problems*, in T. Barth and H. Deconinck, editors, High-Order Methods for Computational Physics, Volume 9 of Lecture Notes in Computational Science and Engineering, Springer, Berlin, 1999, 69-224.

[4] B. Cockburn, S. Hou and C.-W. Shu, *The Runge-Kutta local projection discontinuous Galerkin finite element method for conservation laws IV: the multidimensional case*, Mathematics of Computation, 54 (1990), 545-581.

[5] B. Cockburn, S.-Y. Lin and C.-W. Shu, *TVB Runge-Kutta local projection discontinuous Galerkin finite element method for conservation laws III: one dimensional systems*, Journal of Computational Physics, 84 (1989), 90-113.

[6] B. Cockburn and C.-W. Shu, *TVB Runge-Kutta local projection discontinuous Galerkin finite element method for conservation laws II: general framework*, Mathematics of Computation, 52 (1989), 411-435.

[7] B. Cockburn and C.-W. Shu, *The Runge-Kutta discontinuous Galerkin method for conservation laws V: multidimensional systems*, Journal of Computational Physics, 141 (1998), 199-224.

[8] B. Cockburn and C.-W. Shu, *Runge-Kutta discontinuous Galerkin method for convection-dominated problems*, Journal of Scientific Computing, 16 (2001), 173-261.

[9] M. Dumbser and M. Käser, *Arbitrary high order non-oscillatory Finite Volume schemes on unstructured meshes for linear hyperbolic systems*, Journal of Computational Physics, 221 (2007), 693-723.

[10] O. Friedrichs, *Weighted essentially non-oscillatory schemes for the interpolation of mean values on unstructured grids*, Journal of Computational Physics, 144 (1998), 194-212.

[11] A. Harten, B. Engquist, S. Osher and S. Chakravathy, *Uniformly high order accurate essentially non-oscillatory schemes, III*, Journal of Computational Physics, 71 (1987), 231-303.

[12] J. Hesthaven and T. Warburton, *Nodal Discontinuous Galerkin Methods*, Springer, New York, 2008.

[13] C. Hu and C.-W. Shu, *Weighted essentially non-oscillatory schemes on triangular meshes*, Journal of Computational Physics, 150 (1999), 97-127.

[14] G. Jiang and C.-W. Shu, *Efficient implementation of weighted ENO schemes*, Journal of Computational Physics, 126 (1996), 202-228.

[15] L. Krivodonova, J. Xin, J.-F. Remacle, N. Chevaugeon and J.E. Flaherty, *Shock detection and limiting with discontinuous Galerkin methods for hyperbolic conservation laws*, Applied Numerical Mathematics, 48 (2004), 323-338.

[16] B. Li, *Discontinuous Finite Elements in Fluid Dynamics and Heat Transfer*, Birkhauser, Basel, 2006.

[17] X. Liu, S. Osher and T. Chan, *Weighted essentially non-oscillatory schemes*, Journal of Computational Physics, 115 (1994), 200-212.

[18] H. Luo, J.D. Baum and R. Lohner, *A Hermite WENO-based limiter for discontinuous Galerkin method on unstructured grids*, Journal of Computational Physics, 225 (2007), 686-713.

[19] J. Qiu and C.-W. Shu, *Hermite WENO schemes and their application as limiters for Runge-Kutta discontinuous Galerkin method: one dimensional case*, Journal of Computational Physics, 193 (2003), 115-135.

[20] J. Qiu and C.-W. Shu, *Runge-Kutta discontinuous Galerkin method using WENO limiters*, SIAM Journal on Scientific Computing, 26 (2005), 907-929.

[21] J. Qiu and C.-W. Shu, *A comparison of troubled-cell indicators for Runge-Kutta discontinuous Galerkin methods using weighted essentially nonoscillatory limiters*, SIAM Journal on Scientific Computing, 27 (2005), 995-1013.

[22] J. Qiu and C.-W. Shu, *Hermite WENO schemes and their application as limiters for Runge-Kutta discontinuous Galerkin method II: two dimensional case*, Computers and Fluids, 34 (2005), 642-663.

[23] W.H. Reed and T.R. Hill, *Triangular mesh methods for neutron transport equation*, Tech. Report LA-UR-73-479, Los Alamos Scientific Laboratory, 1973.

[24] J. Shi, C. Hu and C.-W. Shu, *A technique of treating negative weights in WENO schemes*, Journal of Computational Physics, 175 (2002), 108-127.

[25] C.-W. Shu, *TVB uniformly high-order schemes for conservation laws*, Mathematics of Computation, 49 (1987), 105-121.

[26] C.-W. Shu, *Essentially non-oscillatory and weighted essentially non-oscillatory schemes for hyperbolic conservation laws*, in Advanced Numerical Approximation of Nonlinear Hyperbolic Equations, B. Cockburn, C. Johnson, C.-W. Shu, and E. Tadmor, A. Quarteroni, ed., Lecture Notes in Math. 1697, Springer-Verlag, Berlin, 1998, 325-432.

[27] C.-W. Shu, *Discontinuous Galerkin methods: general approach and stability*, in Numerical Solutions of Partial Differential Equations, S. Bertoluzza, S. Falletta, G. Russo

and C.-W. Shu, Advanced Courses in Mathematics CRM Barcelona, Birkhäuser, Basel, 2009, 149-201.

[28] C.-W. Shu and S. Osher, *Efficient implementation of essentially non-oscillatory shock-capturing schemes*, Journal of Computational Physics, 77 (1988), 439-471.

[29] C.-W. Shu and S. Osher, *Efficient implementation of essentially non-oscillatory shock capturing schemes II*, Journal of Computational Physics, 83 (1989), 32-78.

[30] P. Woodward and P. Colella, *The numerical simulation of two-dimensional fluid flow with strong shocks*, Journal of Computational Physics, 54 (1984), 115-173.

[31] Y.-T. Zhang and C.-W. Shu, *Third order WENO scheme on three dimensional tetrahedral meshes*, Communications in Computational Physics, 5 (2009), 836-848.

[32] X. Zhong and C.-W. Shu, *A simple weighted essentially nonoscillatory limiter for Runge-Kutta discontinuous Galerkin methods*, Journal of Computational Physics, 232 (2013), 397-415.

[33] J. Zhu and J. Qiu, *Runge-Kutta discontinuous Galerkin method using WENO type limiters: Three dimensional unstructured meshes*, Communications in Computational Physics, 11 (2012), 985-1005.

[34] J. Zhu, J. Qiu, C.-W. Shu and M. Dumbser, *Runge-Kutta discontinuous Galerkin method using WENO limiters II: Unstructured meshes*, Journal of Computational Physics, 227 (2008), 4330-4353.